

New anomaly observed in ${}^4\text{He}$ supports the existence of the hypothetical X17 particle

A. J. Krasznahorkay ^{1,*}, M. Csatlós ¹, L. Csige ¹, J. Gulyás ¹, A. Krasznahorkay ^{1,†}, B. M. Nyakó ¹,
I. Rajta ¹, J. Timár ¹, I. Vajda ¹ and N. J. Sas ²

¹*Institute for Nuclear Research (ATOMKI), P.O. Box 51, H-4001 Debrecen, Hungary*

²*University of Debrecen, 4010 Debrecen, PO Box 105, Hungary*



(Received 27 October 2019; revised 30 June 2021; accepted 6 October 2021; published 18 October 2021)

Angular correlation spectra of e^+e^- pairs produced in the ${}^3\text{H}(p, e^+e^-){}^4\text{He}$ nuclear reaction have been studied at $E_p = 510, 610, \text{ and } 900$ keV proton energies. The main features of the spectra can be understood by taking into account the internal and external pair creations following the proton capture by ${}^3\text{H}$. However, these processes cannot account for an observed peak around 115° in the angular correlation spectra. This anomalous excess of e^+e^- pairs can be described by the creation and subsequent decay of a light particle during the direct capture process. The derived mass of the particle is $m_{\text{X}17}c^2 = 16.94 \pm 0.12(\text{stat}) \pm 0.21(\text{syst})$ MeV. According to the mass this is likely the same X17 particle, which we recently suggested [Phys. Rev. Lett. **116**, 042501 (2016)] for describing the anomaly observed in the decay of ${}^8\text{Be}$.

DOI: [10.1103/PhysRevC.104.044003](https://doi.org/10.1103/PhysRevC.104.044003)

I. INTRODUCTION

Recently, we measured electron-positron angular correlations for the 17.6 MeV and 18.15 MeV, $J^P = 1^+ \rightarrow J^\pi = 0^+$, $M1$ transitions in ${}^8\text{Be}$ and an anomalous angular correlation was observed [1]. This was interpreted as the creation and decay of an intermediate bosonic particle, which we now call X17, with a mass of $m_{\text{X}17}c^2 = 16.70 \pm 0.35(\text{stat}) \pm 0.5(\text{syst})$ MeV. The possible relation of the X17 boson to the dark matter problem and the fact that it might explain the $(g-2)_\mu$ puzzle, triggered an enhanced theoretical and experimental interest in the particle and hadron physics community [2,3]. A number of such light particles have already been predicted for many decades with a wide range of different properties [4–10], but have never been confirmed experimentally.

Our data were first explained with a 16.7 MeV, vector gauge boson, X17 by Feng and co-workers [11,12], which may mediate a fifth fundamental force with some coupling to standard model (SM) particles. The X17 boson is thus produced in the decay of an excited state to the ground state, ${}^8\text{Be}^* \rightarrow {}^8\text{Be} + \text{X17}$, and then decays through the $\text{X17} \rightarrow e^+e^-$ process. Constraints on such a new particle, were also taken into account by Feng and co-workers [11–13].

Zhang and Miller [14] investigated the possibility to explain the anomaly within nuclear physics. They explored the nuclear transition form factor as a possible origin of the

anomaly, and found the required form factor to be unrealistic for the ${}^8\text{Be}$ nucleus.

Ellwanger and Moretti made another possible explanation of the experimental results through a light pseudoscalar particle [15]. Given the quantum numbers of the ${}^8\text{Be}^*$ and ${}^8\text{Be}$ states, the X17 boson could indeed be a $J^\pi = 0^-$ pseudoscalar particle, if it was emitted with $L = 1$ orbital angular momentum. More recently Wong [16] made a QED2 boson description of such pseudoscalar particle.

Alves and Weiner [17], Alves [18] and Liu [19] revisited experimental constraints on QCD axions in the O(10 MeV) mass window. In particular, they found a variant axion model that remains compatible with existing constraints. This reopens the possibility of solving the strong CP problem at the GeV scale. Such axions or axion-like particles (ALPs) are expected to decay predominantly by the emission of e^+e^- pairs.

Subsequently, many studies with different models have been performed including an extended two Higgs doublet model [20]. Delle Rose and co-workers [21] showed that the anomaly can be described with a very light Z_0 bosonic state. They also showed [22] how both spin-0 and spin-1 solutions are possible and describe beyond the standard model (BSM) scenarios.

The X17 boson is expected to decay promptly into e^+e^- pairs, which then could be detected inside the experimental setup. The decay rate is determined by their coupling constant to electrons (ϵ_e). A comprehensive discussion of the constraints regarding to ϵ_e of X17 can be found in Ref. [23]. Combining them with the most recent results of the NA64 collaboration [24], one can get the following limits: $6.8 \times 10^{-4} \leq \epsilon_e \leq 2 \times 10^{-3}$.

In parallel to these recent theoretical studies, there are several experiments (MEGII [25], Darklight [26], SHiP [27], and others [28]) planning to search for the X17 boson, and large collaborations like BESIII and BelleII [29,30], NA64

*kraszna@atomki.hu

†Present address: CERN, Geneva, Switzerland

Published by the American Physical Society under the terms of the [Creative Commons Attribution 4.0 International](https://creativecommons.org/licenses/by/4.0/) license. Further distribution of this work must maintain attribution to the author(s) and the published article's title, journal citation, and DOI.

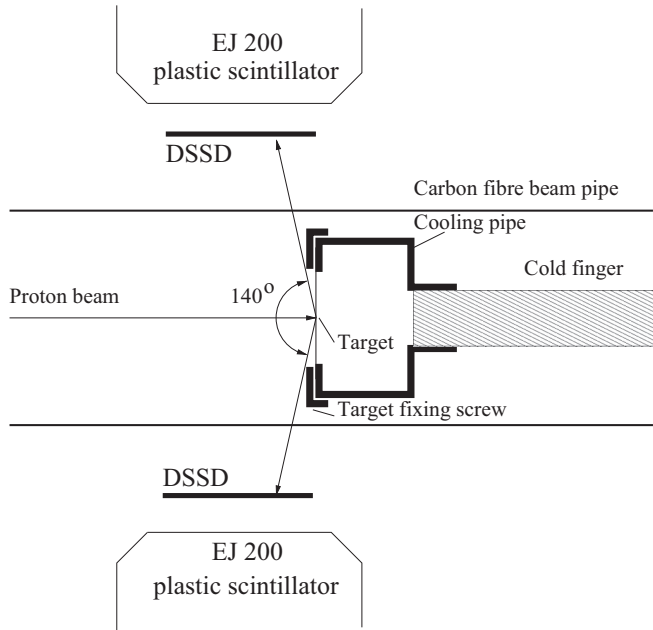


FIG. 1. Schematic drawing of the target cooling system.

[24], PADME [31] NICA [32], and others are dedicating part of their efforts to clarify the X17 issue.

We also reinvestigated the ^8Be anomaly with an improved experimental setup. We have confirmed the signal of the assumed X17 particle and measured its mass and branching ratio with improved precision [33,34]. The observed deviation in the angular correlation of the e^+e^- pairs was found much smaller in the 17.6 MeV than in the 18.15 MeV transition of ^8Be [35].

II. EXPERIMENTS

In the present work, we have conducted a search for the X17 particle in the $^3\text{H}(p, \gamma)^4\text{He}$ reaction using different proton beam energies. The experiment was performed in Debrecen at the 2 MV Tandetron accelerator of ATOMKI. The $^3\text{H}(p, \gamma)^4\text{He}$ reaction was used at proton bombarding energies of $E_p = 510, 610, \text{ and } 900$ keV. This would induce direct capture [36] and resonant capture and populate the overlapping $J^\pi = 0^+$ first, and $J^\pi = 0^-$ second excited states in ^4He [37].

The proton beam with a typical current of $1.0 \mu\text{A}$ was impinging on a ^3H target for about 100 h for each bombarding energy. The ^3H was absorbed in a 4.2 mg/cm^2 thick Ti layer evaporated onto an 0.4 mm thick molybdenum disk with a diameter of 50 mm . The density of the ^3H atoms was $\approx 2.7 \times 10^{20} \text{ atoms/cm}^2$. The disk was cooled down to liquid N_2 temperature to prevent ^3H evaporation. In such a thick $^3\text{H}+\text{Ti}$ target, the proton beam was stopped completely. The target was shifted off the center of the spectrometer by 25 mm downstream along the proton beam axis to avoid the screening by the target backing and holder. We have used a large (50 mm diameter) cooling pipe with a fixing screw, which limited the maximal correlation angle to $\approx 140^\circ$, since the surface of the target was inside the pipe as is shown in Fig. 1.

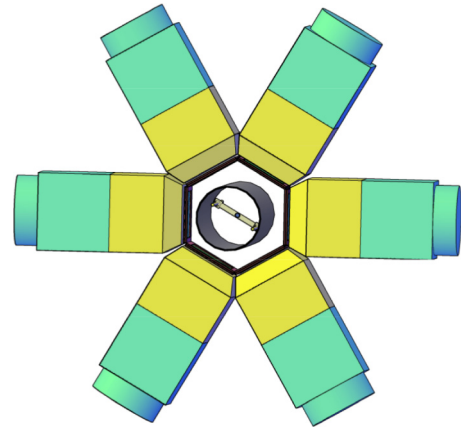


FIG. 2. CAD drawing of the e^+e^- spectrometer. The target (black/blue spot in the center of the figure) is evaporated onto $10 \mu\text{m}$ Al strip foil spanned between 3 mm thick Perspex rods to minimize the scattering and external pair creation in the vicinity of the target. The beam pipe is shown in black around which the DSSD detectors are arranged. The scintillators are shown in yellow while their light guides are in green. The PMT tubes are not shown.

The proton energies were chosen to stay below the threshold of the (p, n) reaction ($E_{\text{thr}} = 1.018 \text{ MeV}$). The ^4He nucleus was excited up to $E_x = 20.21, 20.29, \text{ and } 20.49 \text{ MeV}$ at the used proton beam energies, so it was expected that the first excited state of ^4He ($J^P = 0^+, E_x = 20.21 \text{ MeV}, \Gamma = 0.50 \text{ MeV}$) and the second one ($J^P = 0^-, E_x = 21.01 \text{ MeV}, \Gamma = 0.84 \text{ MeV}$) were both populated [37].

III. THE SPECTROMETER

Our previous experimental setup [1,38] has recently been upgraded by the replacement of the scintillators with EJ200 ones and PM tubes by Hamamatsu 10233-100 ones. The sizes of the scintillators were $82 \times 86 \times 80 \text{ mm}^3$ each. The schematic arrangement of the detectors is shown in Fig. 2.

As another improvement, the multiwire proportional chambers (MWPC) have been replaced by novel double-sided silicon strip detectors (DSSD), placed very close to the front face of the scintillators, to enhance the efficiency of the experimental setup and its homogeneity.

As shown in Fig. 2, we also increased the number of telescopes from five to six. The positions of the hits were registered by the DSSDs having sizes of $50 \times 50 \text{ mm}^2$, strip widths of 3 mm and a thickness of $500 \mu\text{m}$. The telescope detectors were perpendicular to the beam direction, each at 60° to its neighbors, around a vacuum chamber made of a carbon fiber tube with a wall thickness of 1 mm , shown in black in Fig. 2. The target shown in the figure is just used for calibration. The real ^3H cooled target's geometry was discussed before.

A. Trigger for data readout and data acquisition

The signals from the photomultipliers of the E detectors are processed in constant fraction discriminator units (CF8000). The CFD thresholds are adjusted slightly above the noise level. The CFD unit supplied a multiplicity signal,

whose amplitude was proportional to the number of detector hits. This signal was then fed into a fast discriminator unit requiring multiplicity-2 coincidences. In order to allow the simultaneous measurement of single telescope events, a trigger box was set to allow a scaled-down fraction of single telescope events as well.

The signals from the DSSD detectors were processed with a 16 channel preamplifier, shaper and discriminator units with multiplexed readout (MUX-16). Up to two simultaneously responding channels were identified and the two amplitudes plus the two corresponding amplitude coded addresses were sent to the bus. These units are especially well suited for DSSD single or double hit applications. The unit also provided ORed signals of the timing discriminators.

Time and energy signals of the scintillators, as well as the time, energy and position signals of the DSSD detectors were recorded.

B. Energy and position calibrations of the spectrometer

The energy calibration of the telescopes for low energies was made with the Compton edges of a ^{60}Co source.

We also performed experiments using the $^7\text{Li}(p, \gamma)^8\text{Be}$ reaction, which produced high energy transitions. As in our previous measurements, with $E_p = 441$ keV this 17.6 MeV transition provided us with a well-known and theoretically interpretable γ -ray and e^+e^- -pair spectra.

First we selected events in which both particles were detected by the same telescope, and lost their energies in the same scintillator. Such events were identified by the double hits in the DSSD detectors. The 6.05 MeV and 17.6 MeV peaks were clearly visible in the spectra generated, allowing us to perform the energy calibration of each scintillator.

In order to determine the x and y coordinates of the hits in the DSSD detectors we used a special preamplifier, shaper, discriminator with multiplexed readout unit designed for those detectors, called MUX-16 and produced by mesytec GmbH. It gives “position” outputs proportional to the strip number (position) 22.2 mV increment per strip. These signals were fed into ADC units. Using a pulse generator input of the MUX-16 unit, the selected channel address cycles around and produces a “fence” spectrum with peaks corresponding to the different strips of the DSSD detectors. Similar spectrum is produced, with the same peak positions, when the real DSSD detector gives signal to the unit. However, if some strips did not work properly, the corresponding peak is missing from the spectrum and cannot be used for calibrations. That is reason we used both type of calibrations for the DSSD detectors.

The energy calibration of the DSSD detectors were performed by using Compton edges of γ rays from a ^{60}Co source. According to those calibrations the thresholds of the discriminators were set uniformly to 50 keV, which was just above the noise level. The average energy loss of electrons and positrons was found to be only 150 keV in the DSSD detectors, so setting the detection thresholds precisely was important.

The setup of the coincidence time gates between the plastic scintillators and their corresponding DSSD detectors was also performed using the data of the calibration experiment.

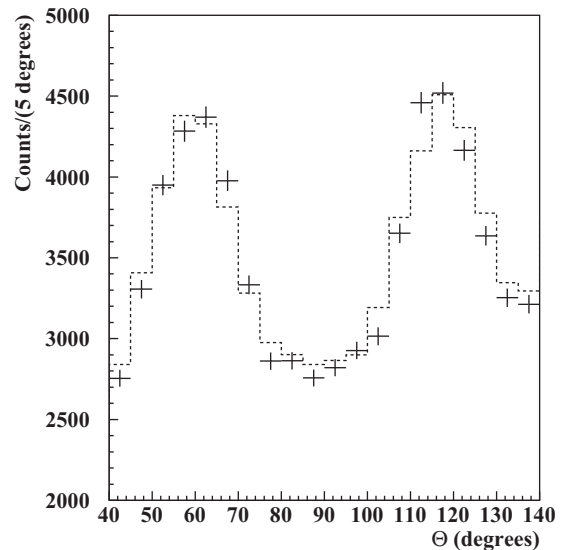


FIG. 3. Detector response for the setup as a function of correlation angle (θ) for isotropic emission of e^+e^- pairs (solid line crosses) compared with the results of the Monte Carlo simulations (dashed line histogram) as explained in the text.

C. Efficiency calibration of the spectrometer

It was crucial for the precise angular correlation measurements to measure and understand the response of the whole detector system to isotropic e^+e^- pairs as a function of the correlation/opening angle. We were aiming at a precision of a few % for the shape of the response function.

The detectors measure continuous e^+e^- spectra and the sum of the energies are constructed off-line. Due to the energy loss in the wall of the vacuum chamber and in the DSSD detectors, as well as the finite thresholds of the discriminators (CFD), the low-energy part of the spectrum is always cut out. Since we measure e^+e^- coincidences, such a low energy cut also means a high energy cut for the particles detected in coincidence. Thresholds were set to have similar efficiencies in the different telescopes. After a proper energy calibration of the telescopes, this was done in the analysis software. The response curve was found to depend primarily on the geometrical arrangement of the detector telescopes.

Beside the e^+e^- coincidences, down-scaled single events were also collected during the whole run of the experiment for making acceptance/efficiency calibrations. An event mixing method [39] was used to experimentally determine the relative response of the spectrometer as a function of the correlation angle by using the single telescope triggered events. Uncorrelated lepton pairs were generated from subsequent single events and their correlation angle was calculated as for the coincident events. The resulting angular correlation for the uncorrelated events gave us the experimental response curve. Reasonably good agreement was obtained to the results of the Monte Carlo simulations, as presented in Fig. 3. The average difference is within $\approx 3.0\%$ in the 40° – 170° range.

When electrons from the target pass through the setup to the DSSD detectors, multiple scattering in the target holder, in the wall of the carbon fiber vacuum chamber, and in the DSSD

detectors itself can take place. This gives rise to spread in the reconstructed angular correlation. The simulated angular resolution corresponds to $\text{FWHM} \approx 7^\circ$. We hence use bins of 5° in the correlation spectra.

The shape of the coincidence response curve depends also on the position of the beam spot, which may walk during a long experiment. However, using the above event mixing method, this effect can be compensated, so the extracted angular correlation would be independent of small variations in the beam spot position.

IV. MONTE CARLO SIMULATIONS

Simulations of the experiment were performed by GEANT3 [40], taking the full experimental setup into account. This included the target, its backing, the target holder, and all materials in the vicinity of the target and the detectors; the packaging of the detectors, the light guides and the various pieces used to mount the detectors.

The computer simulation of particles traversing the experimental setup takes into account the interactions of those particles with the material of the detector. GEANT is able to simulate the dominant processes which can occur in the energy range from 10 keV to 10 TeV for electromagnetic interactions.

The length of the detector telescopes was large enough (80 mm) to stop almost all 20 MeV electrons or positrons. The γ radiations created by bremsstrahlung or annihilation could in some cases escape from the detectors, resulting in distorted peak shapes.

The simulation follows the tracks of the primary electrons and positrons through the set-up, together with secondary particles induced by γ s, including the annihilation γ s. The detected energy losses in the scintillators are kept track of, including the kinetic energy that is left over at the end of a track when the particle stopped inside the scintillator. These idealized signals from the detectors are analyzed in the same way as the calibrated data.

e^+e^- pairs from E/M IPC transitions were generated for the detector simulation according to the Rose calculations [41]. e^+e^- pairs from a hypothetical intermediate boson decay could also be generated, as well as background processes like γ - γ coincidences, single high energy γ events, and traversing cosmic muons.

A. Validating the results of the simulations

In order to test the accuracy of these—naturally not perfect—simulations for describing our experiments, we made measurements with the previously described ${}^7\text{Li}(p, \gamma){}^8\text{Be}$ reaction.

First a ${}^7\text{Li}$ target evaporated onto a thin ($10\mu\text{m}$) Al strip was used in the same place where we put the ${}^3\text{H}$ target later on. The experimental results for the angular correlations from this data taking with $E_p = 441$ keV (dots with error bars) are shown in Fig. 4, together with the corresponding IPC Monte Carlo simulation (histogram) coming mostly from the $M1$ nuclear transition. The contribution coming from the external pair creation (EPC) of the 17.6 MeV γ rays is shown by a

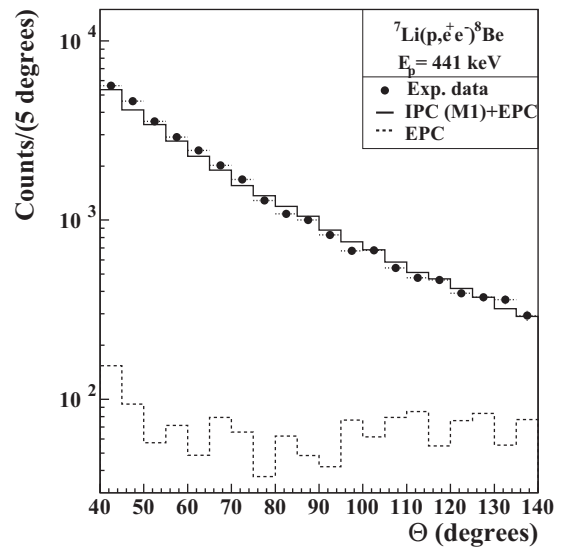


FIG. 4. e^+e^- angular correlations obtained for the 17.6 MeV transition of ${}^8\text{Be}$ by using thin target backing.

dashed line histogram. We note here that the direct capture contribution is negligible compared to the $M1$ IPC due to the large resonance capture cross section. The ratio of the event numbers used for the simulations are determined by the internal pair creation coefficient of the 17.6 MeV $M1$ transition.

As can be seen in Fig. 4, the simulation of this single (IPC) process manages to describe the shape of the data distribution accurately, and the contribution of EPC created on the different parts of the spectrometer is reasonably low.

In the next step a ${}^7\text{Li}$ target was evaporated onto the same Ti+Mo backing that the ${}^3\text{H}$ target used, in the same geometrical setup as described earlier. Since the internal pair creation coefficient calculated by Viviani *et al.* [42] for ${}^4\text{He}$ is only slightly higher than that calculated for the 17.6 MeV transition in ${}^8\text{Be}$, this transition allowed us to accurately test the backgrounds coming from γ radiation in our main experimental setup as well. The results from that data taking are shown in Fig. 5.

The ratio of the event numbers used for the simulations are determined by the internal pair creation coefficient as described before. A fit of these IPC+EPC simulations to the data are also shown in Fig. 5, providing an accurate description of the experimental data. The contribution of the IPC and EPC processes to the events selected by our analysis in this case is about the same.

These results convinced us that our spectrometer's behavior could be accurately described by our simulations, even in the presence of intense γ rays and a thick target backing.

V. EXPERIMENTAL RESULTS

In order to search for the assumed X17 particle, both the energy-sum spectrum of the e^+e^- pairs measured by the telescopes, and their angular correlations, determined by the DSSD detectors, have been analyzed. For the real “signal” events we always required that the energy-sum for the

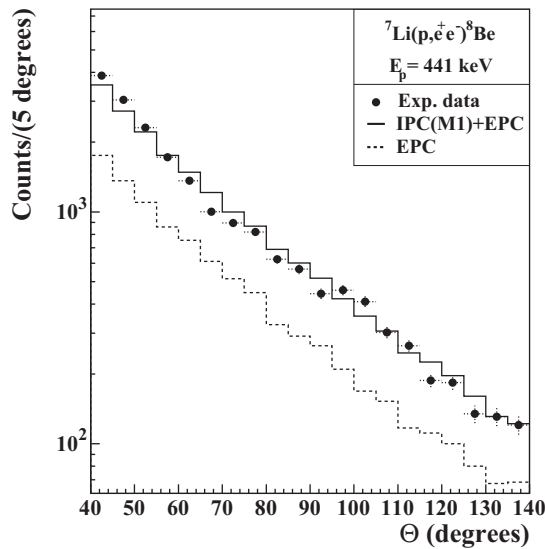


FIG. 5. e^+e^- angular correlations obtained for the 17.6 MeV transition of ${}^8\text{Be}$ by using thick target backing.

e^+e^- pairs should be equal to the transition energy, which we want to investigate.

Since the counting rates in the detectors were low (≈ 150 Hz in the scintillators and ≈ 25 Hz in the DSSD detectors) and the coincidence time window was sharp (≈ 10 ns), the effect of random coincidences was negligible. In the following, we show only the real-coincidence gated spectra.

The downscaled ($\times 0.08$) energy-sum spectrum of the e^+e^- pairs collected by all combinations of the telescope pairs in the 10–25 MeV energy range is shown by a dashed-line histogram in Fig. 6(a) after subtracting the cosmic-ray background (CRB). This background was measured for two weeks before and after the experiments using the same gates and conditions as used for the in-beam data. It has been found that above $E(\text{sum}) = 25$ MeV only the CRB contributes to the spectrum.

The CRB contribution in the studied 10–25 MeV energy range has been determined by normalizing the off-beam spectrum to the in-beam spectra in the energy range $E(\text{sum}) \geq 25$ MeV. This contribution has been found to be a relatively small part of the total spectrum as indicated by the dotted histogram in Fig. 6(a). In the figure, $E(\text{sum})$ means the measured energy sum of the e^+ and e^- particles corrected for the energy loss due to the pair creation (1.02 MeV) and for the average energy loss of the two particles when crossing the vacuum chamber and the DSSD detectors (1.08 MeV).

In order to reduce the external pair creation (EPC) background, we constructed a spectrum also from e^+e^- pairs, which were detected by telescope pairs with relative angles of 120° . The spectrum is shown in Fig. 6(a) as a full-line histogram. The general shape of this histogram is similar to that of the dashed-line one, however there is a well observable peak on top of the smoothly decreasing shape at around 20.5 MeV. The difference of the two spectra is presented in Fig. 6(b). The peak in the spectrum may come from the internal pairs created in the direct proton capture process or in

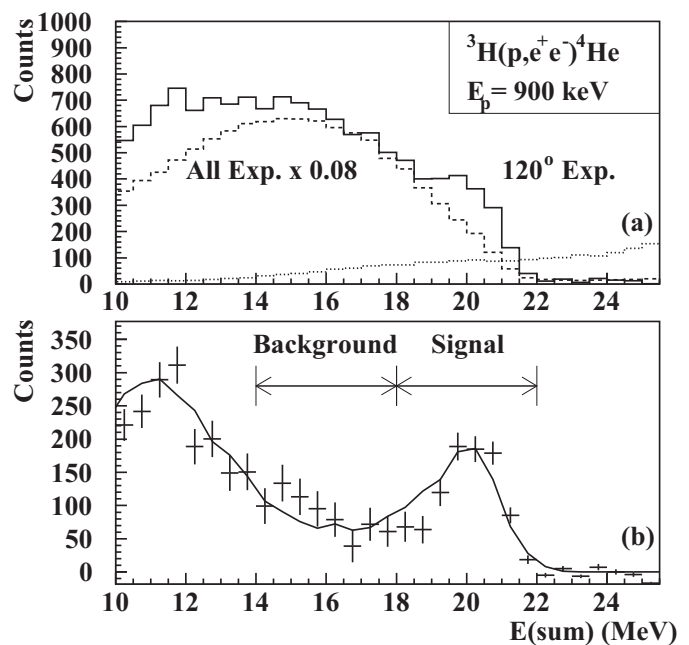


FIG. 6. (a) Experimental energy-sum spectra of the e^+e^- pairs derived, respectively, for “All” different detector combinations (dashed-line histogram with counts multiplied by 0.08) and for detectors at 120° relative angles (solid-line histogram). The cosmic-ray background contributions are subtracted from both spectra. The CRB spectrum corresponding to the “All” spectrum is plotted with dotted line. (b) The markers with error bars show the difference of the solid-line and dashed-line distributions from (a). The solid line represents the same difference, calculated using the simulated response of the spectrometer for γ rays (through external e^+e^- pair creation) created in the direct proton capture on ${}^3\text{H}$, and for the e^+e^- pairs expected from the decay of the hypothetical X17 particle.

the $0^+ \rightarrow 0^+$ $E0$ transition of ${}^4\text{He}$ and may also come from the e^+e^- decay of the X17 hypothetical particle. The background in the spectrum below $E(\text{sum}) = 17$ MeV is created by external pairs induced by the γ rays coming from the direct proton capture on the ${}^3\text{H}$ target.

To check these possibilities, in the further analysis we have compared the angular correlation spectra of the e^+e^- pairs corresponding to this peak region [“Signal” in Fig. 6(b)] with that of obtained for the background region [“Background” in Fig. 6(b)]. The angular correlations of the e^+e^- pairs were determined from the position data of the DSSD detectors for each beam energy.

The angular correlation spectra obtained for ${}^4\text{He}$ are indicated in Fig. 7 by dots, stars, and full circles for $E_p = 510$, 610, and 900 keV, respectively. For better readability, the spectra are shifted by 1-1 orders of magnitude according to the labels.

The angular correlations of the e^+e^- pairs for the background region marked in Fig. 6 are shown in Fig. 8, similarly to Fig. 7.

The experimental angular correlations were compared to combinations of Monte Carlo simulations of different processes resulting in valid e^+e^- events in the spectrometer. An

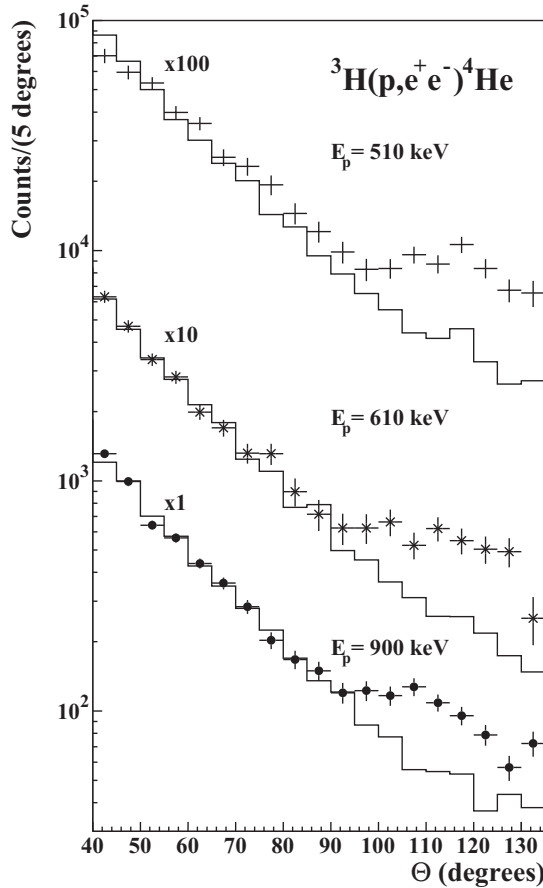


FIG. 7. Angular correlations of the e^+e^- pairs for the “Signal” region (see Fig. 6). Symbols with error bars indicate experimental data measured in the ${}^3\text{H}(p, \gamma){}^4\text{He}$ reaction at different proton beam energies, while solid-line histograms correspond to the respective data obtained in the simulations described in the text.

e^+e^- event is considered valid, if it passed all the conditions and cuts that was applied for the experimental data.

In the light of the above considerations, we also simulated the contribution of the external e^+e^- pairs created by the high-energy γ rays from the ${}^3\text{H}(p, \gamma){}^4\text{He}$ reaction. We also determined the contribution of the internal pair creation (IPC) process. For that, both the properties of the proton capture process and the emission of an e^+e^- pair mediated by a one-photon exchange was calculated by Viviani and co-workers [42]. They provided us with high-statistic Monte Carlo event files which we used as particle generator inputs in our GEANT3 simulations.

The simulated angular correlations are indicated by full-line histograms in Figs. 7 and 8 for the “Signal” and the “Background” sum-energy ranges, respectively.

We found that the most significant background was provided by e^+e^- pairs created by γ rays generated during direct proton capture on ${}^3\text{H}$. For small correlation angles, this process can fully interpret the measured values. As a result of this, the normalization of the contribution of γ events was derived from the simulation’s fit to the data in the 40° to 70° opening angle region.

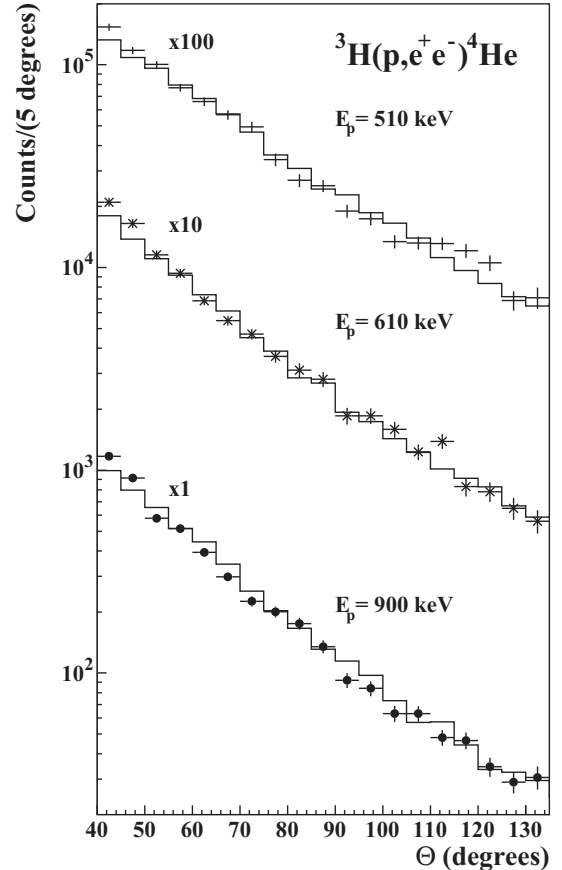


FIG. 8. Angular correlations of the e^+e^- pairs for the “Background” region (see Fig. 6). See the caption of Fig. 7 for more details.

Note that for the background regions of the sum energy, the experimental and the corresponding simulated curves show a fairly good agreement over the entire angular range (see Fig. 8), thus validating the correctness of the simulations.

Here, we mention that in this case the usual method of background determination, i.e., performing the experiment without target material, cannot be applied because the main source of the background is the target material itself.

For further theoretical interpretation of the results shown in Fig. 7, the simulated angular correlations were subtracted from the experimental ones. The angular correlations (points with error bars) obtained after subtraction are shown in Fig. 9.

The corresponding proton beam energies are indicated in the figure. The anomaly previously observed and explained by the decay of the X17 particle appeared at each of the bombarding energies.

A. Fitting the angular correlations

In order to derive the exact value for the mass of the decaying particle from the present data, we carried out a fitting procedure for both the mass value and the amplitude of the observed peak.

The fit of the original experimental data was performed with ROOFIT [43] by describing the e^+e^- angular correlation

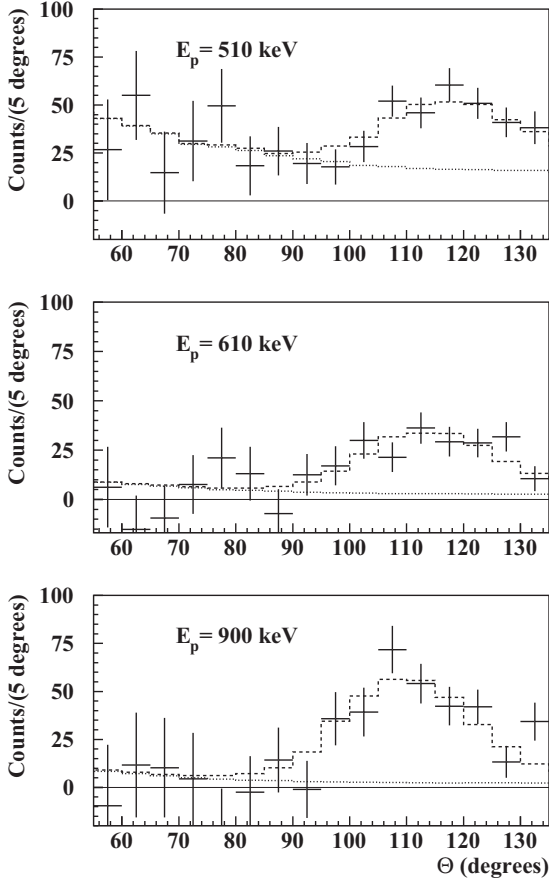


FIG. 9. Comparison of the experimental and the simulated angular correlations of the e^+e^- pairs. The best fitted sum (dashed line) as sum of the the simulated background (dotted line) and the simulated contribution of the hypothetical X17 boson is compared with the experimental signal values (dots with error bars).

with the following intensity function (*INT*):

$$\begin{aligned} INT = & N_{\text{EPC}} \times PDF(\text{EPC}) + N_{\text{IPC}} \times PDF(\text{IPC}) \\ & + N_{\text{Sig}} * PDF(\text{sig}), \end{aligned} \quad (1)$$

where $PDF(X)$ stands for the MC-simulated probability density function and N_X is the fitted number of the events of the given process. $PDF(\text{sig})$ was simulated by GEANT3 incorporating the relativistic two-body decay of a particle with a given mass. Therefore, $PDF(\text{sig})$ was constructed as a two-dimensional model as a function of the e^+e^- opening angle and the mass of the simulated particle. To construct the mass dependence, the PDF linearly interpolates the e^+e^- opening angle distributions simulated for discrete particle masses.

Using the intensity function described in Eq. (1), we first performed a list of fits by fixing the simulated particle mass in the signal PDF to a certain value, and employing ROOFIT to estimate the best values for N_{Sig} , N_{EPC} , and N_{IPC} . Allowing the particle mass to vary in the fit, the best fitted mass is calculated. We also made the fits by fixing the N_{EPC} value to the experimental data as described earlier.

The values obtained for the energy and branching ratio of the X17 boson and the IPC values, as a result of the average of

TABLE I. Internal pair creation coefficients (IPCC), X17 boson branching ratios (B_x), masses of the X17 particle, and confidences derived from the fits.

E_p (keV)	IPCC $\times 10^{-4}$	B_x $\times 10^{-6}$	Mass (MeV/ c^2)	Confidence
510	2.5(3)	6.2(7)	17.01(12)	7.3σ
610	1.0(7)	4.1(6)	16.88(16)	6.6σ
900	1.1(11)	6.5(20)	16.68(30)	8.9σ
Averages		5.1(13)	16.94(12)	
^8Be values		6	16.70(35)	

the two fits described above, are summarized in Table I, and the corresponding fits after subtraction of the EPC background are shown in Fig. 9.

B. Systematic uncertainties

The systematic uncertainties were estimated from the simulations. Taking into account the uncertainty of the target position along the beam line estimated to be ± 2 mm, may cause an $\Delta m_{Xc^2} = \pm 0.06$ MeV uncertainty. The uncertainty of the position of the beam spot perpendicular to the beam axis was estimated to be ± 2 mm in the worst case, which may cause a shift in the invariant mass of $\Delta m_{Xc^2} = \pm 0.15$ MeV. The total systematic error was conservatively estimated as $\Delta m_{Xc^2}(\text{syst}) = \pm 0.21$ MeV.

VI. CONCLUSIONS ON X17

Table I shows the fitting parameters and the average of the parameters. As can be seen, consistent values were obtained for each fitting parameter. In the last row, our corresponding values measured in the case of ^8Be are also shown [1].

The obtained mass agrees very well with that observed in the earlier ^8Be experiment [$m_{Xc^2} = 16.70 \pm 0.35(\text{stat}) \pm 0.5(\text{syst})$ MeV], which is remarkable considering that the excesses in the observed angular correlation spectra appear at different correlation angles as one would indeed expect from the kinematics of the relativistic two-body decay. Therefore, our new observation enhances the possibility that the measured anomalies can be attributed to the same new particle X17.

As shown, the branching ratios of the X17 particle are identical within uncertainties, for the three beam energies proving that the X17 particle was most likely formed in direct proton capture, which has a dominant multipolarity of $E1$.

As discussed, IPC is generated mostly during the direct capture ($E1$) transition, however, the IPCC was found to be much smaller than expected from the Bohr's approximation and also smaller than the one predicted by Viviani and co-workers [42].

Very recently, Zhang and Miller [44] studied the protophobic vector boson explanation by deriving an isospin relation between photon and X17 couplings to nucleons. They concluded that X17 production is dominated by direct capture transitions both in ^8Be and ^4He without going through any nuclear resonance. A smooth energy dependence is predicted

that occurs for all proton beam energies above threshold [44]. Our present results obtained for ${}^4\text{He}$ at different beam energies agrees with their prediction.

VII. SUMMARY

We have studied the energy-sum and angular correlation spectra of e^+e^- pairs produced in the ${}^3\text{H}(p, \gamma){}^4\text{He}$ reaction at $E_p = 510, 610, \text{ and } 900$ keV proton energies. The main features of the spectra can be understood rather well taking into account the internal and external pair creations following the direct proton capture on the target. We have, however, observed a peak-like anomalous excess of e^+e^- pairs in the angular correlation spectra around 115° at each beam energy. This e^+e^- excess cannot be accounted for by the above processes, however, it can be described by the creation and subsequent decay of a light particle, created during

the proton capture process to the ground state of the ${}^4\text{He}$ nucleus. The derived mass of the particle [$m_{\text{X}c^2} = 16.94 \pm 0.12(\text{stat}) \pm 0.21(\text{syst})$ MeV] agrees well with that of the X17 particle, which we recently suggested [1,33,34] for describing the anomaly observed in ${}^8\text{Be}$.

ACKNOWLEDGMENTS

We wish to thank M. Viviani for providing us with their theoretical results, D. Horváth for the critical reading of the manuscript and for the many useful discussions. We wish to thank also Gy. Zilizi for providing us with the ${}^3\text{H}$ targets, Z. Pintye for the mechanical, and J. Molnár for the electronic design of the experiment. This work has been supported by the Hungarian National Research, Development and Innovation Office NKFIH Grants No. K124810 and by the GINOP-2.3.3-15-2016-00034 and GINOP-2.3.3-15-2016-00005 grants.

-
- [1] A. J. Krasznahorkay *et al.*, *Phys. Rev. Lett.* **116**, 042501 (2016).
 [2] A. Datta, J. Feng, S. Kamali, and J. Kumar, *Phys. Rev. D* **101**, 035010 (2020).
 [3] Citations for Ref. [1]: <https://inspirehep.net/literature?sort=mostrecent&size=25&page=1&q=refersto%3Arecid%3A1358248>.
 [4] S. Weinberg, *Phys. Rev. Lett.* **40**, 223 (1978).
 [5] F. Wilczek, *Phys. Rev. Lett.* **40**, 279 (1978).
 [6] T. W. Donnelly, S. J. Freedman, R. S. Lytel, R. D. Peccei, and M. Schwartz, *Phys. Rev. D* **18**, 1607 (1978).
 [7] P. Fayet, *Phys. Rev. D* **70**, 023514 (2004).
 [8] M. Pospelov, A. Ritz, and B. Voloshin, *Phys. Lett. B* **662**, 53 (2008).
 [9] C.-Y. Wong, *Phys. Rev. C* **81**, 064903 (2010).
 [10] H. Davoudiasl, H.-S. Lee, and W. J. Marciano, *Phys. Rev. D* **85**, 115019 (2012).
 [11] J. L. Feng, B. Fornal, I. Galon, S. Gardner, J. Smolinsky, T. M. P. Tait, and P. Tanedo, *Phys. Rev. Lett.* **117**, 071803 (2016).
 [12] J. L. Feng, B. Fornal, I. Galon, S. Gardner, J. Smolinsky, T. M. P. Tait, and P. Tanedo, *Phys. Rev. D* **95**, 035017 (2017).
 [13] B. Fornal, *Int. J. Mod. Phys. A* **32**, 1730020 (2017).
 [14] X. Zhang and G. A. Miller, *Phys. Lett. B* **773**, 159 (2017).
 [15] U. Ellwanger and S. Moretti, *J. High Energy Phys.* **11** (2016) 039.
 [16] C.-Y. Wong, *J. High Energy Phys.* **08** (2020) 165.
 [17] D. S. M. Alves and N. J. Weiner, *J. High Energy Phys.* **07** (2018) 092.
 [18] D. S. M. Alves, *Phys. Rev. D* **103**, 055018 (2021).
 [19] J. Liu, N. McGinnis, C. E. M. Wagner, and X.-P. Wang, *J. High Energy Phys.* **05** (2021) 138.
 [20] L. D. Rose, S. Khalil, and S. Moretti, *Phys. Rev. D* **96**, 115024 (2017), and references therein.
 [21] L. Delle Rose, S. Khalil, S. J. D. King, S. Moretti, and A. M. Thabt, *Phys. Rev. D* **99**, 055022 (2019).
 [22] L. D. Rose, S. Khalil, S. King, and S. Moretti, *Front. Phys.* **7**, 73 (2019).
 [23] J. Kozaczuk, D. E. Morrissey, and S. R. Stroberg, *Phys. Rev. D* **95**, 115024 (2017).
 [24] E. Deoero *et al.* (NA64 Collaboration), *Eur. Phys. J. C* **80**, 1158 (2020).
 [25] A. M. Baldini *et al.* (MEGII Collaboration), *Eur. Phys. J. C* **78**, 380 (2018).
 [26] J. Balewski *et al.*, [arXiv:1412.4717](https://arxiv.org/abs/1412.4717).
 [27] C. Ahdida *et al.* (SHIP Collaboration), *J. High Energy Phys.* **04** (2021) 199.
 [28] M. Battaglieri *et al.*, [arXiv:1707.04591](https://arxiv.org/abs/1707.04591).
 [29] E. Kou, P. Urquijo, W. Altmannshofer *et al.* (Belle-II Collaboration), *Prog. Theor. Exp. Phys.* **2019**, 123C01 (2019); **2020**, 029201 (2020).
 [30] K. Ban, Y. Jho, Y. Known *et al.*, *J. High Energy Phys.* **04** (2021) 091.
 [31] G. Piperno (PADME Collaboration), *J. Instrum.* **15**, C05008 (2020).
 [32] E. Kokoulina, N. Barlikov, A. Gribowsky *et al.*, *J. Phys.: Conf. Ser.* **1690**, 012035 (2020).
 [33] A. J. Krasznahorkay *et al.*, *J. Phys.: Conf. Ser.* **1056**, 012028 (2017).
 [34] A. J. Krasznahorkay *et al.*, *Acta Phys. Pol. B* **50**, 675 (2019).
 [35] A. J. Krasznahorkay *et al.*, Proceedings of Science (Bormio2017) 036 (2017).
 [36] K. I. Hahn, C. R. Brune, and R. W. Kavanagh, *Phys. Rev. C* **51**, 1624 (1995).
 [37] D. R. Tilley, H. R. Weller, and G. M. Hale, *Nucl. Phys. A* **541**, 1 (1992).
 [38] J. Gulyás *et al.*, *Nucl. Instrum. Methods Phys. Res. A* **808**, 21 (2016).
 [39] S. Ravan, P. Pujahari, S. Prasad, and C. A. Pruneau, *Phys. Rev. C* **89**, 024906 (2014).
 [40] R. Brun, F. Bruyant, M. Maire, A. C. McPherson, and P. Zancarini, GEANT3 User's guide, Report No. CERN-DD-EE-84-01 (1987).
 [41] M. E. Rose, *Phys. Rev.* **76**, 678 (1949); **78**, 184 (1950).
 [42] M. Viviani *et al.*, [arXiv:2104.07808](https://arxiv.org/abs/2104.07808).
 [43] W. Verkerke and D. P. Kirkby, The ROOFIT toolkit for data modeling, eConf C **0303241**, MOLT007 (2003) [physics/0306116].
 [44] X. Zhang and G. A. Miller, *Phys. Lett. B* **813**, 136061 (2021).